

Phase diagram of the mixed-spin (1,3/2) Ising ferrimagnetic system with two different anisotropies

D. C. da Silva,^{*} A. S. de Arruda,[†] and M. Godoy[‡]

Instituto de Física, Universidade Federal de Mato Grosso, 78060-900, Cuiabá, MT, Brazil.

(Dated: December 15, 2021)

Abstract

In this work, we have performed Monte Carlo simulations to study phase transitions in a mixed spin-1 and spin-3/2 Ising ferrimagnetic system on the square and cubic lattices and with two different single-ion anisotropies. This lattice is divided in two interpenetrating sublattices with spins $S^A = 1$ (states ± 1 and 0) on the sublattice A and $S^B = 3/2$ (states $\pm 3/2, \pm 1/2$) on the sublattice B . We have used single-ion anisotropies D_A and D_B acting on the sites of the sublattice A and B , respectively. We have determined the phase diagrams of the model in the temperature T versus the single-ion anisotropies strength D_A and D_B plane and shown that the system exhibits both second- and first-order phase transitions. We also have shown that this system displays compensation points for some values of the anisotropies.

^{*} davidcristiano@fisica.ufmt.br

[†] aarruda@fisica.ufmt.br

[‡] mgodoy@fisica.ufmt.br

I. INTRODUCTION

The study of mixed-spin models has its importance recognized because they are related to ferrimagnetic materials [1–3]. In these models, the particles that carry two different spins are distributed in two interpenetrating sublattices. Then each pair nearest-neighbor spins are coupled antiferromagnetically so that at low temperatures all the spins are allied antiparallel. Thus, in each sublattice, there is a magnetization, both with different magnitudes and opposite signs. Therefore, the system as a whole presents a magnetization (total magnetization). When the temperature is increased, the spins of the different sublattices have their alignments decreased. Then, at a certain temperature, these alignments inverted of the magnetic moments are compensated, causing the total magnetization goes to zero for a temperature smaller than the critical temperature (T_c). This temperature is called the compensation temperature (T_{comp}). Materials that present this behavior are known as ferrimagnets. The compensation temperature becomes the ferrimagnet system of great interest for technological applications [4–6] because in this point the coercive field has great growth [7, 8], so a small driving field is necessary to change the signal of the resulting magnetization.

Most ferrimagnetic materials have been modeled by mixed-spins Ising model through a variety of combinations of two spins (σ, S), i.e., $(1/2, 1)$, $(1/2, 3/2)$, $(1, 3/2)$, and so on. It is important to note that the critical behavior is the same for both ferromagnetic ($J > 0$) and ferrimagnetic ($J < 0$) systems [9]. There are exact solutions [10–13] for the simplest case $(1/2, 1)$. Kaneyoshi *et al.* [14, 15] and Plascak *et al.* [16] provided theoretical investigations of magnetic properties and the influence of a single-ion anisotropy in the compensation temperature (T_{comp}) of a bipartite ferrimagnets such as $MnCu(pba - OH)(H_2)_3$. These spin systems have been investigated using a variety of approaches, such as effective-field theory [17–24], mean-field approximation [9, 25–29], renormalization-group [30], numerical Monte Carlo simulations [31–33]. In particular, the model that presents the combination of spins ($S_1 = 1$ and $S_2 = 3/2$) has been too much studied, so that there is synthesized material $[NiCr_2(bipy)_2(C_2O_4)_4(H_2O)]H_2O$, which indicates a very rare case of the existence of antiferromagnetism between Ni with $S = 1$ and Cr with $S = 3/2$ [34]. On the other hand, from the theoretical point of view, Abubrig *et al.* [9] and Souza *et al.* [25] performed mean-field studies and showed that the complete phase diagram exhibited a tricritical behavior and compensation points.

In this paper, we are interested to study the phase diagram, giving a greater emphasis on the first-order phase transitions. We have also looked for occurrences of compensation temperatures by using Monte Carlo simulations. Thus, we have inspired in the work of Pereira *et al.* [35] who performed Monte Carlo simulations to study a mixed spin-1 and spin-3/2 Ising ferrimagnetic system on a square lattice with two different random single-ion anisotropies. They have determined the phase diagram of the model in the temperature versus strength random single-ion anisotropy plane showing that it exhibits only second-order phase transition lines, and they also have shown that this system displays compensation temperatures for some cases of the random single-ion distribution. Here, using a case more complete we have shown that the system also presents first-order phase transition and tricritical behavior.

The paper is organized as follows: in Section II, we have described the mixed spin-1 and spin-3/2 ferrimagnetic system and we present some details concerning the simulation procedures. In Section III, we have shown the results obtained. Finally, in the last Section IV, we have presented our conclusions.

II. THE MODEL AND SIMULATIONS

The mixed spin-1 and spin-3/2 Ising ferrimagnetic system consists of two interpenetrating square and cubic sublattices A , with spin-1 (states $S^A = 0, \pm 1$), and B with spin-3/2 (states $S^B = \pm 1/2, \pm 3/2$). In each site of the sublattices, there are single-ion anisotropies D_A and D_B acting on the spin-1 and spin-3/2, respectively. This system is described by the following Hamiltonian model,

$$\mathcal{H} = -J \sum_{\langle i,j \rangle} S_i^A S_j^B + D_A \sum_{i \in A} (S_i^A)^2 + D_B \sum_{j \in B} (S_j^B)^2, \quad (1)$$

where the first term represents the interaction between the nearest neighbors spins on sites i and j located on the sublattices A and B , respectively. J is the magnitude of the exchange interaction, and the sum is over all nearest neighboring pairs of spins. J may be either antiferromagnetic, $J < 0$, as assumed often for ferrimagnets, or ferromagnetic, $J > 0$. Both cases are completely equivalent by a simple spin reversal on either sublattice. Here, for the reason of simplicity, we have considered the case ferromagnetic exchange interaction, $J > 0$ in our simulations. As a consequence, in our case, the magnetizations of both sublattices are identical at the compensation point, while in the antiferromagnetic case,

at the same compensation point, the sublattice magnetizations have equal magnitude but different sign leading to the above-mentioned vanishing the total magnetization before the critical temperature [36]. The second and third terms represent the single-ion anisotropies D_A and D_B at all the sites of the sublattices A and B , respectively. Therefore, the sum is only performed over $N/2$ spins of the sublattices A and B .

The magnetic properties of the system have been studied using Monte Carlo simulations. In our simulations were used lattice sizes ranging from $L = 16$ up to 128 for the square lattice and from $L = 8$ up to 32 for the cubic lattice. These lattices consist of two interpenetrating sublattices, each one containing $L^2/2$ (square lattice) and $L^3/2$ (cubic lattice) sites with periodic boundary conditions. The initial states of the system were prepared randomly and updated by the Metropolis algorithm [37]. We used 10 independent samples for any size lattice, but as the error bars are smaller than the symbol sizes, we do not show it in the figures. Typically, we used 3.0×10^5 MCs (Monte Carlo steps) for the calculation of average values of thermodynamic quantities of interest, after discarding 1.0×10^5 MCs for thermalization, for both square and cubic system. Here, 1 MCs means $N = L^2$ (square lattice) or L^3 (cubic lattice) trials to change the state of a spin of the lattice. The temperature is measured in units J/k_B (equal 1.0 for all simulations) and the anisotropies are measured in units J/zk_B , where z is the coordination number and $z = 4$ for the square and $z = 6$ for cubic lattices.

We have calculated the sublattice magnetizations per site, m_A and m_B , defined as

$$m_A = \frac{2[\langle M_A \rangle]}{N} = \frac{2[\langle \sum_A S_i^A \rangle]}{N}, \quad (2)$$

and

$$m_B = \frac{2[\langle M_B \rangle]}{N} = \frac{2[\langle \sum_B S_j^B \rangle]}{N}, \quad (3)$$

where $\langle \dots \rangle$ denotes thermal averages and $[\dots]$ denotes average over the samples of the system. The order parameter is the total magnetization per site m_T defined as

$$m_T = \frac{[\langle M \rangle]}{N} = \frac{[\langle M_A + M_B \rangle]}{N} = \frac{|m_A + m_B|}{2}. \quad (4)$$

Therefore, we defined another parameter that is convenient to obtain the compensation point, which is given by

$$m_S = \frac{[\langle M \rangle]}{N} = \frac{[\langle M_A - M_B \rangle]}{N} = \frac{|m_A - m_B|}{2}. \quad (5)$$

Further, we also have calculated the following thermodynamics quantities, the specific heat per site

$$C_e = \frac{[\langle E^2 \rangle] - [\langle E \rangle]^2}{k_B T^2 N}, \quad (6)$$

where k_B is the Boltzmann constant and E the total energy of the system. The susceptibility is denoted by χ :

$$\chi = \frac{[\langle M_T^2 \rangle] - [\langle M_T \rangle]^2}{k_B T N}, \quad (7)$$

In order to find the critical point, we used the total U fourth-order Binder cumulant [38] defined by:

$$U = 1 - \frac{[\langle M_T^4 \rangle]}{3[\langle M_T^2 \rangle]^2}, \quad (8)$$

The transition temperature also can be estimated by the position of the peaks of the response functions C_e and χ , but to obtain with greater accuracy in some cases, we have used the intersection of the curves of fourth-order Binder cumulants for different lattice sizes L .

The parameter m_S vanishes at the compensation point [39]. Then, the compensation point can be determined by looking at the point where the sublattice magnetizations would coincide. We also require that the compensation point occurs for temperatures below T_c , where T_c is the critical temperature.

III. RESULTS AND DISCUSSIONS

A. Ground-state

We begin by presenting the ground-state diagram of the system. The ground-state is similar to the obtained by Abubrig et al. and Nakamura [9, 40], but in our case we have used in the Hamiltonian of the system the sign plus for D_A and D_B (see Eq. 1) and the exchange parameter is $J > 0$. At zero temperature, we have found four phases with different values of $\{m_A, m_B, q_A, q_B\}$, namely the ordered ferrimagnetic phases $F_I \equiv \{1, 3/2, 1, 9/4\}$ (or $F_I \equiv \{-1, -3/2, 1, 9/4\}$), $F_{II} \equiv \{1, 1/2, 1, 1/4\}$ (or $F_{II} \equiv \{-1, -1/2, 1, 1/4\}$) and the disordered phases $P_I \equiv \{0, 0, 0, 9/4\}$ and $P_2 \equiv \{0, 0, 0, 1/4\}$, where the parameters q_A and q_B are defined by $q_A = \langle (S_i^A)^2 \rangle$ and $q_B = \langle (S_j^B)^2 \rangle$.

Therefore, the ground-state phase diagram is easily obtained from Hamiltonian (Eq. 1) by comparing the ground-state energies of the different phases and we have shown in Fig. 1.

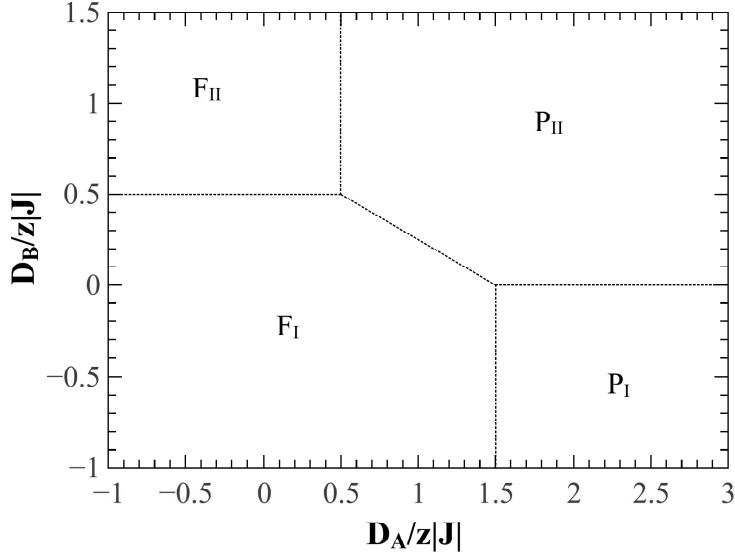


FIG. 1. Ground-state diagram of the mixed spin-1 and spin-3/2 Ising ferrimagnetic system with two different single-ion anisotropies $D_A/z|J|$ and $D_B/z|J|$. The four phases: ordered F_I , F_{II} and disordered P_I , P_{II} are separated by lines of first-order transitions.

All the phases are separated by lines of first-order transitions represented by dotted lines and the values of the coordinates are obtained independently of the coordination number z . For an interesting case, on the line $D_B/z|J| = 0.5$, we have F_I and F_{II} coexisting phases. On the other hand, for very small temperatures (for example $T \approx 0.1$) the sublattice magnetizations are $m_A \cong 1.0$ and $m_B \cong 1.5$ (see Fig. 8(a) and (b)) and when the temperature increases they go together continuously to zero. Thus, we will call this phase of the ordered phase F .

B. Phase diagram for the case $D = D_A/J = D_B/J$

We also have calculated the phase diagram in the $D - T$ plane for the mixed spin-1 and spin-3/2 Ising ferrimagnetic system on the square and cubic lattice, and for the case $D = D_A/J = D_B/J$, as shown in Fig. 2. Our results obtained on the square lattice are similar to the obtained by Žukovič and Bobák [41], but with the difference that here we have used in the Hamiltonian (see Eq. 1) sign plus for $D = D_A/J = D_B/J$ and the exchange parameter is $J > 0$. The phase diagram exhibits only second-order phase transitions between the ordered F_I and disordered P phases on the square (circle-solid line) and cubic (square-solid line) lattices.

In order to observe the finite-size behavior of the magnetic properties of the system, we have calculated the total magnetization m_T (Fig. 3(a)), the fourth-order cumulant U_L (Fig. 3(b)), the specific heat C_e (Fig. 3(c)) and the susceptibility χ_L (Fig. 3(d)) as a function of temperature T and for different lattice sizes, as indicated in Fig. 3.

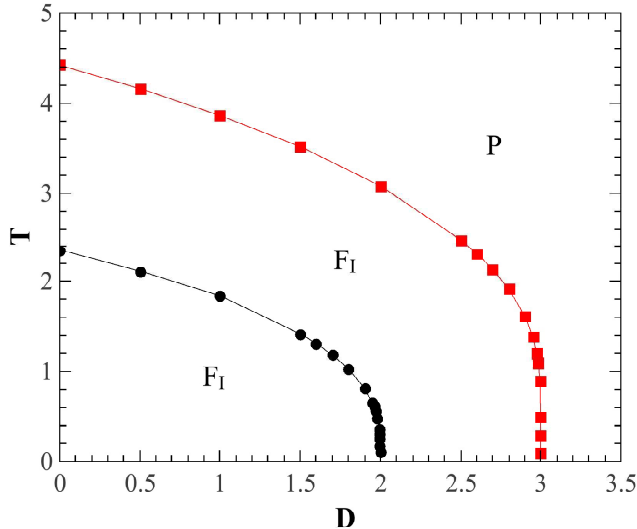


FIG. 2. (Color online) Phase diagram in the $D - T$ plane for mixed spin-1 and spin-3/2 Ising ferrimagnetic system on the square and cubic lattices. Here, we considered the case $D = D_A = D_B$. The circle- (square lattice) and square-solid (cubic lattice) lines denote second-order phase transitions.

The transition points can be estimated from the locations of the peaks of the specific heat C_e and of the susceptibility χ_L . To find the critical points with higher precision, we can use the intersection of the fourth-order cumulant U_L curves for different lattice size (see Fig. 3(b)) [38]. Thus, we obtained the value of critical temperature with $D = 0$, as $T_c = 2.354 \pm 0.003$ (square lattice), where this value is in good agreement with one found in the reference [41]. We also obtained $T_c = 4.419 \pm 0.002$ on the cubic lattice with $D = 0$. To find the coordinates of the points in the transition lines for high temperatures (see Fig. 2 for $1.0 \leq T < T_c(D = 0)$), we have used the peaks of the susceptibility as a function of temperature T . On the other hand, in the region of low temperatures ($0 < T \lesssim 1.2$) the phase boundary is almost vertical to the D -axis, instead of the temperature dependencies of various thermodynamic functions it is more convenient to look into their single-ion parameter D dependencies at a fixed temperature T . Therefore, we have used the

peaks of the susceptibility χ as a function of the anisotropy D for a T fixed. In all simulations, we have used $L = 128$ and $L = 32$ on the square and cubic lattices, respectively.

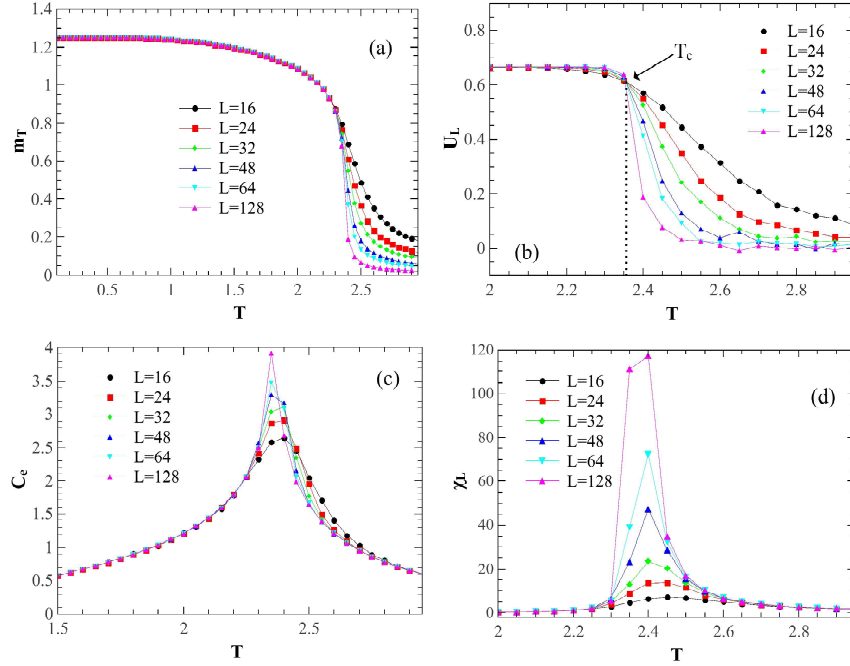


FIG. 3. (Color online) (a) Total magnetization m_T , (b) fourth-order cumulant U_L , (c) specific heat C_e and (d) susceptibility χ_L as a function of temperature T and for different lattice sizes, as indicated in the figures. Here, we considered the case $D = 0$.

We also have verified the existence of a compensation point as a function of the single-ion anisotropy strength D on the square (Fig. 4(a)) and cubic (Fig. 4(c)) lattices. In Fig. 4(a) (square lattice), we can observe that there is no compensation point for $D < 1.954$. On the other hand, for values in the range of $1.954 < D \leq 1.970$ we have found always two compensation points and in the range of $1.970 < D < 2.0$ the system exhibits only one compensation point. To confirm, we have plotted the staggered magnetization m_s versus temperature T , and for different values of D , where we can observe the two compensation points (see Fig. 4(b)). Now, for the case of the cubic lattice (see Fig. 4(c)) we did not find any compensation point for $D < 2.9067$ whereas in the range of $2.9067 \leq D \leq 2.9147$ found two compensation points and in the range of $2.9147 < D < 3.0$ only one compensation point. Here, we also have plotted the staggered magnetization m_s versus single-ion anisotropy strength D , and for different values of T , as shown in Fig. 4(d). The system exhibits a compensation point.

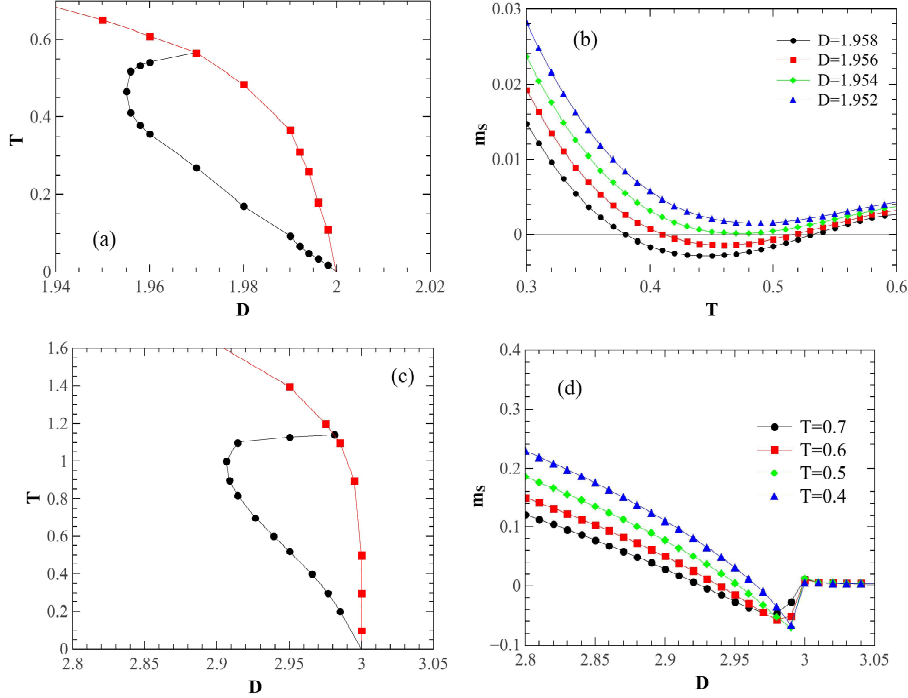


FIG. 4. (Color online) Temperature T versus single-ion anisotropy strength D on the square (a) and cubic (c) lattices. The square-solid lines denote the second-order transition lines and the circle-solid lines are compensation points. (b) Staggered magnetization m_s versus temperature T for different values of D , as shown in the figure. (d) Staggered magnetization m_s versus single-ion anisotropy strength D for different values of T , as shown in the figure. All results were obtained for $L = 128$ (square lattice) and $L = 32$ (cubic lattice).

C. Phase diagram for the case D_B fixed

Let us now consider the case in which D_B is fixed. In Fig. 5(a), we have presented the phase diagram in the $D_A - T$ plane for the system only on the square lattice, and for different values of D_B in the range of $0 < D_B < 2.50$. Therefore, in Fig. 5(a) is possible concluded that all phase transitions are second-order phase transitions between the ordered F_I and disordered P phases for $D_B \leq 0$, and between the ordered F_{II} and disordered P phases for $D_B \geq 2.5$. On the other hand, we have second- and first-order transitions between the F_I and P phases in the range of $0 < D_B < 2.0$. In this region, the ordered F_I phase is separated from the disordered P phase by a line of phase transitions, which change at the tricritical point from second- to first-order. We calculated the coordinates of the tricritical points which are represented by star-dots, for example, the coordinates for some points

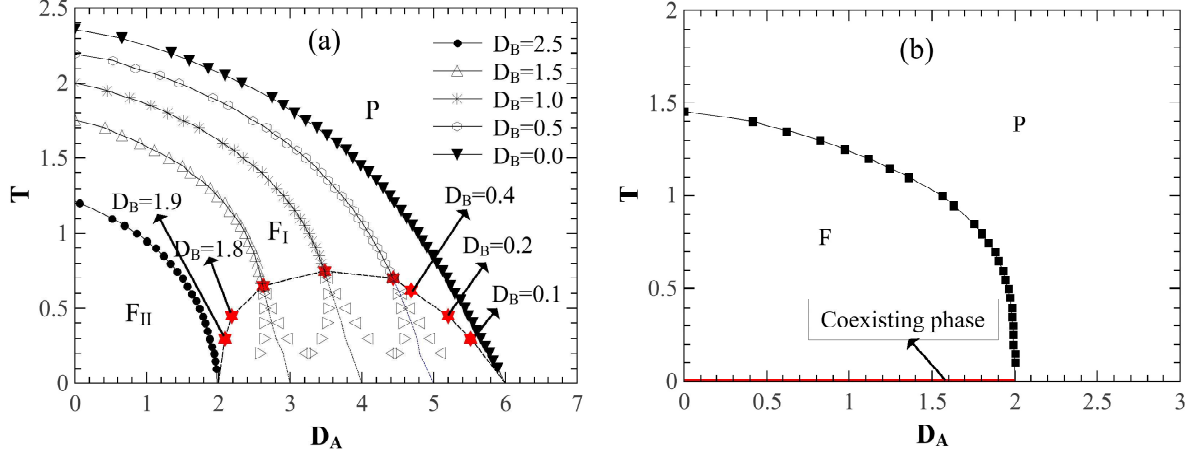


FIG. 5. (Color online) (a) Phase diagram in the D_A – T plane for the mixed spin-1 and spin-3/2 Ising ferrimagnetic system on the square lattice, and for different values of D_B , as shown in the figure. All the full lines are second-order phase transitions. The empty triangles denote the hysteresis widths at first-order transitions between F_I and P phases with the expected phase transition boundary represented by the dotted lines. F_I , F_{II} are the ordered phases and P is a disordered phase. (b) Phase diagram for the special case $D_B = 2.0$, where F is an ordered phase and the solid line (for $T = 0$) is the F_I and F_{II} coexisting phase.

are: with $D_B = 1.50$ ($D_A^t = 2.62$, $T^t = 0.65$), $D_B = 1.0$ ($D_A^t = 3.48$, $T^t = 0.75$) and $D_B = 0.50$ ($D_A^t = 4.43$, $T^t = 0.70$). Thus, we can observe that there is a tricritical points line which is represented by a star-dotted line in the phase diagram. This line is in the range of $0.10 \leq D_B \leq 1.90$. In Fig. 5(b), we exhibited the phase diagram for the special case $D_B = 2.0$ where we have defined F (ferrimagnetic phase) as an ordered phase different from F_I and F_{II} . The solid line (see D_A -axis for $T = 0$) represents the coexistence from the F_I and F_{II} phases.

Now looking at the transition between the two phases F_I and P for low-temperature, Fig. 5(a). We presented in Fig. 6 the total magnetization m_T as increasing (∇) and decreasing (\triangle) functions of D_A one can observe their discontinuous character and the appearance of hysteresis loops, the widths of which increase with decreasing temperature T . Therefore, an expected first-order transition boundary is obtained by a simple linear interpolation between the estimated tricritical and the exact ground-state transition points (square-dots) and only serves as a guide to the eye. We obtained these results for $D_B = 0.50$ (Fig. 6(a)), 1.00 (Fig.

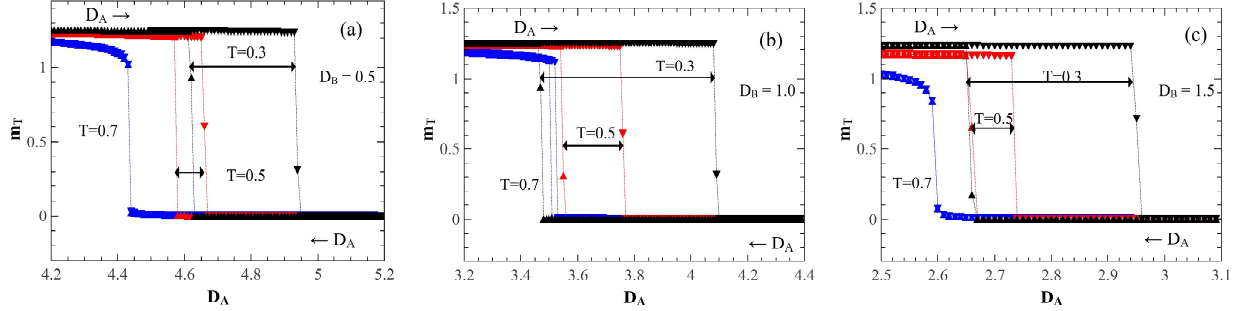


FIG. 6. (Color online) Hysteresis of the total magnetization m_T as a function of increasing (∇) and decreasing (\triangle) single-ion anisotropy D_A and for several values of T fixed indicated in the figures. (a) It is for an anisotropy fixed $D_B = 0.5$, (b) for 1.0 and (c) for 1.5. Here, we have used $L = 128$ (square lattice) and the double-headed arrows denote the loop hysteresis widths. The dotted lines are a guide to the eyes.

6(b)) and 1.50 (Fig. 6(c)). We have used $L = 128$ (square lattice) and the double-headed arrows denote the loop hysteresis widths.

D. Phase diagram for the case D_A fixed

Finally in this section, we exhibited the phase diagram in the $D_B - T$ plane for the system only on the square lattice and different values of D_A , as shown in Fig. 7 and 9. Firstly, the phase diagrams of Fig. 7(a) with $D_A = 1.0$, Fig. 7(b) with $D_A = 0$ and Fig. 7(c) with $D_A = -2.0$ we found only second-order phase transitions from the ordered F_I and F_{II} to disordered P phases, and between the ordered F_I to F_{II} phases. We also calculated the compensation points which are represented by triangle-solid lines.

It is important now to examine the behavior of the sublattice magnetizations m_A and m_B in the second-order phase transition regions and in order to verify the phase diagrams presented in Fig. 7. However, we have restricted our study to the behavior of the magnetization only for one value of the parameter $D_A = 1.0$ (Fig. 7(a)). Thus, the behavior of m_A and m_B , in these transitions, are shown in Fig. 8. In Fig. 8(a) and (b) we exhibited the behavior m_A and m_B as a function of the anisotropy D_B for several values of T . In the range of $0 \leq T \leq 0.2$ the sublattice magnetizations are constants $m_A = 1.0$ and $m_B = 1.5$ in the F_I phase ($D_B \leq 2.0$, see Fig. 7). When the temperature increases $m_A = 1.0$ no

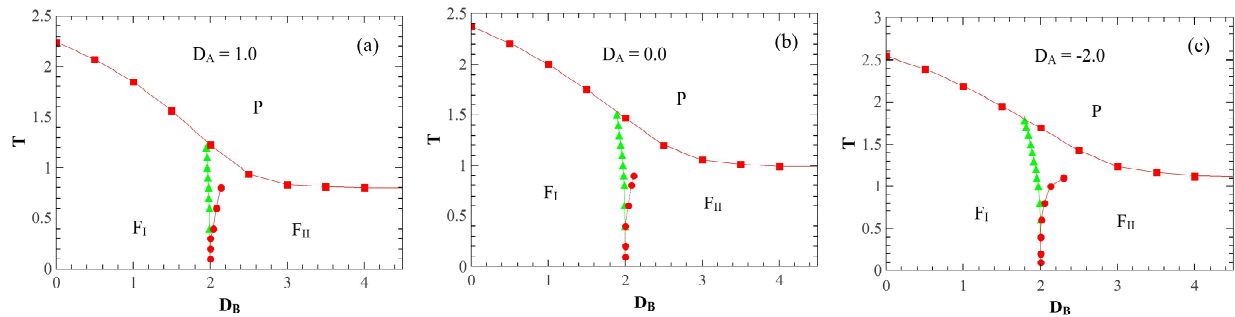


FIG. 7. (Color online) Phase diagram in the $D_B - T$ plane for the mixed spin-1 and spin-3/2 Ising ferrimagnetic system on the square lattice for different values of D_A , as shown in the figures: (a) for $D_A = 1.00$, (b) 0 and (c) -2.00. All the square- and circle-solid lines are second-order phase transition. F_I and F_{II} are ordered phases and P is a disordered phase. The triangle-solid lines are the compensation points.

change and m_B changes quickly for $m_B = 0.5$ now in the F_{II} phase ($D_B > 2.0$). This fact indicates that the system preserves the characteristics of the ground-state phases. On the other hand, in the range of $0.2 < T \leq 0.8$, the sublattice magnetizations are $m_A \approx 1.0$ and $m_B \approx 1.5$ in the F_I phase and they go to any value $0 < m_A < 1.0$ and $0 < m_B < 0.5$ in the F_{II} phase. This transition line, $F_I - F_{II}$ ends at the critical end point which the coordinate are: for $D_A = 1.0$ ($D_B^e = 2.14, T_e = 0.80$), $D_A = 0$ ($D_B^e = 2.11, T_e = 0.90$) and $D_A = -2.0$ ($D_B^e = 2.30, T_e = 1.10$). Now, for $T > 0.9$ the m_A and m_B start in the F_I phase, cross to the F_{II} phase and after go to P phase, as for example, we can see in the curve for $T = 1.0$, Figs. 8(a) and (b).

We also can observe the behavior sublattice magnetizations in the transition line F_I, F_{II} to P . The temperature dependence of the m_A and m_B and for several values of D_B are shown in Figs. 8(c) and (d), respectively. For $T < T_c$ the m_B has a re-entrant behavior, as can see for $D_B = 2.1$ and $D_B = 2.5$ in Fig. 8(d). For this case, we have a competition between the parameters J, D_A, D_B , and T which makes it difficult to align the sublattice magnetization and also due to the finite-size effects in low-temperature. When the temperature is increased ($T \rightarrow T_c$), the system passes from the F_{II} phase to the F_I phase and goes to zero in the P phase.

Another region of the phase diagram which also is important, but it was not presented in Fig. 7, is shown in Fig. 9 for values of $D_A \geq 2.0$ as indicated in the figure. For values

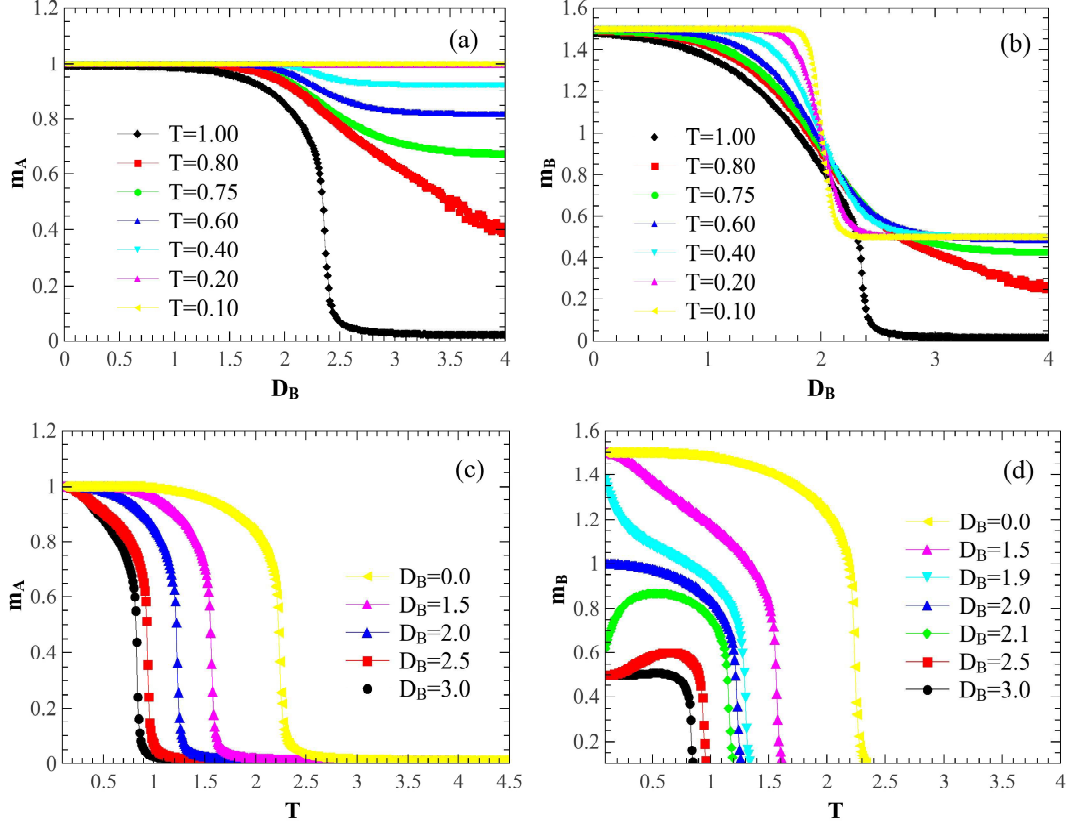


FIG. 8. (Color online) Sublattice magnetizations m_A (a) and m_B (b) as a function of the anisotropy D_B for several values of T , as indicated in the figures. Sublattice magnetizations m_A (c) and m_B (d) as function of temperature T for several values of D_B , as indicated in the figures. Here, we have used a lattice size $L = 128$ (square lattice) and fixed $D_A = 1.0$.

of D_B between 0 and 2.0, we also have second- and first-order phase transition lines linked by a tricritical point and they separate the F_I phase from the P phase. We have connected these points by a line (star-dotted line) and showed that there is a small region where all the phase transition lines are first-order. We also can observe in the phase diagram that the empty triangles represent the hysteresis loop widths at first-order transitions between F_I and P phases. This transition line was obtained using the same procedure as in the previous section and the expected phase transition boundary is denoted by a dotted line.

In Fig 10, we exhibited the hysteresis loop of the total magnetization m_T as a function of increasing (∇) and decreasing (Δ) single-ion anisotropy D_B and for several values of temperatures T fixed indicated in the figures. Fig. 10(a) is for an anisotropy fixed $D_A = 3.0$, Fig. 10(b) for $D_A = 4.0$ and the Fig. 10(c) for $D_A = 5.0$. These plots show a characteristic

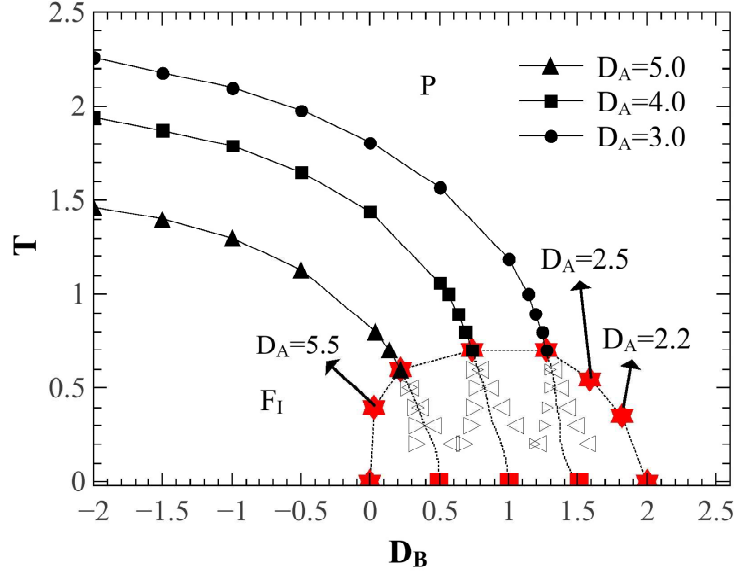


FIG. 9. (Color online) Phase diagram in the $D_B - T$ plane for the mixed spin-1 and spin-3/2 Ising ferrimagnetic system on the square lattice, and different values of D_A indicated in the figure. All the full lines are second-order phase transitions. The empty triangles denote the hysteresis widths at first-order transitions between F_I and P phases with the expected phase transition boundary represented by the dotted lines. The star-dotted line represents a tricritical points line. The F_I and P are the ordered and disordered phases, respectively.

behaviors in first-order transitions, such as the discontinuities in the magnetizations.

IV. CONCLUSIONS

In this work, we have studied the mixed-spin Ising model with ferrimagnetic interaction between spin-1 (states $\pm 1, 0$) and spins-3/2 (states $\pm 1/2, \pm 3/2$). We performed Monte Carlo simulations on the square and cubic lattices, where each type of spin is fixed in a sublattice and with anisotropies D_A and D_B on the respective sublattices A and B. Firstly, we studied a particular case of model in which the anisotropies are equal, $D = D_A/J = D_B/J$. This case was studied by Zukovic *et al.* [41] on the square lattice and they showed that the system presents only second-order phase transition. We also found only second-order phase transitions for both square and cubic lattices between the ordered F and disordered P phases, and a multi-compensation point behavior, i.e., with two compensation points for the same value of anisotropy D (see Fig. 4(a) and (c)). In the case of anisotropy D_B fixed,

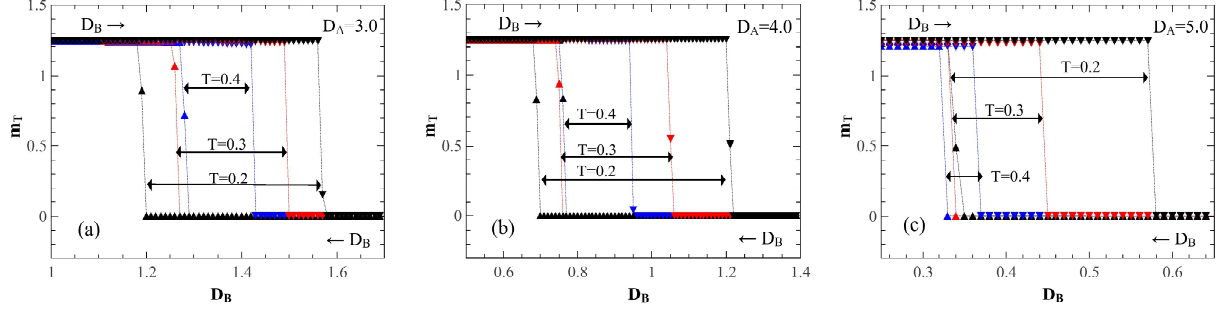


FIG. 10. (Color online) Hysteresis loop of the total magnetization m_T as a function of increasing (∇) and decreasing (\triangle) single-ion anisotropy D_B and for several values of temperatures T fixed indicated in the figures. (a) It is for an anisotropy fixed $D_A = 3.0$, (b) for 4.0 and (c) for 5.0. Here, we have used $L = 128$ (square lattice) and the double-headed arrows denote the loop hysteresis widths. The dotted lines are a guide to the eyes.

the phase diagram presents two different ferrimagnetic phases, F_I and F_{II} . In the range of $0 < D_B < 2.0$, we found first- and second-order phase transitions between the ordered F_I and the disordered P phases, i.e., the system presents a tricritical behavior. On the other hand, in the range of $-\infty \leq D_B \leq 0$ and $2.0 < D_B < \infty$ we have found only second-order phase transitions between the $F_I - P$ and $F_{II} - P$ phases, respectively (see Fig. 5). We also observe that in this case, the model does not exhibit compensation points.

Now, for the case of fixed D_A , but in the range of $-\infty < D_A < 2.0$ (see Fig. 7), we observe second-order phase transitions between the ordered F_I and F_{II} phases for low-temperatures $T \leq 0.3$, where the system preserves the characteristics of the ground-state phases ($T = 0$). When we increase the temperature $T > 0.3$ (the system no more preserves the characteristic of the ground state). The system continuous exhibiting second-order phase transitions between the $F_I - F_{II}$ phases (see Fig. 8) where the phase F_I is defined as a region with $m_A \neq 0$ ($0 < m_A < 1.0$) and $m_B \neq 0$ ($0 < m_B < 1.5$) and F_{II} a region with $m_A \neq 0$ ($0 < m_A < 1.0$) and $m_B \neq 0$ ($0 < m_B < 0.5$) for different temperature values T and for any value of $D_B > 2.0$. We also found second-order phase transitions between the phases: $F_I - P$ and $F_{II} - P$. We also observed first- and second-order phase transitions between phase F_I and phase P , in the range of $2.0 < D_A < 6.0$ (see Fig. 9), i.e., it presents a tricritical behavior with a tricritical points line.

V. ACKNOWLEDGMENTS

The authors acknowledge financial support from the Brazilian agencies CNPq and CAPES.

-
- [1] T. Mallah, S. Thiebaut, M. Verdaguer, and P. Veillet, *Science* **262**, 1554 (1993).
 - [2] H. Okawa, N. Matsumoto, H. Tamaki, and M. Ohba, *Mol. Cryst. Liq. Cryst.* **233**, 257 (1993).
 - [3] C. Mathoniere, C. J. Nutall, S. G. Carling, and P. Day, *Inorg. Chem.* **35**, 1201 (1996).
 - [4] M. Mansuripur, *J. Appl. Phys.* **61**, 1580 (1987).
 - [5] H. P. D. Shieh and M. H. Kryder, *Appl. Phys. Lett.* **49**, 473 (1986).
 - [6] O. Kahn, *Molecular Magnetism*, (VCH, New York, 1993).
 - [7] P. Hansen, *J. Appl. Phys.* **62**, 216 (1987).
 - [8] G. M. Buendia and E. Machado, *Phys. Rev. B* **61**, 14686 (2000).
 - [9] O. F. Abubrig, D. Horvath, and A. Bobak, M. Jascur, *Physica A* **296**, 437 (2001).
 - [10] L. L. Goncalves, *Phys. Scripta* **32**, 248 (1985).
 - [11] A. Lipowski and T. Horiguchi, *J. Phys. A: Math. Gen.* **28**, L261 (1995).
 - [12] M. Jascur, *Physica A* **252**, 217 (1998).
 - [13] A. Dakhama, *Physica A* **252**, 225 (1998).
 - [14] T. Kaneyoshi and Y. Nakamura, *J. Phys.: Condens. Matter* **10**, 3003 (1998).
 - [15] T. Kaneyoshi and Y. Nakamura, S. Shin, *J. Phys.: Condens. Matter* **10**, 7025 (1998).
 - [16] H. F. Verona de Resende, F. C. Sá Barreto, and J. A. Plascak, *Physica A* **149A**, 606 (1988).
 - [17] T. Kaneyoshi, *J. Phys. Soc. Japan* **56**, 2675 (1987).
 - [18] T. Kaneyoshi, *Physica A* **153**, 556 (1988).
 - [19] T. Kaneyoshi, *J. Magn. Magn. Mat.* **92**, 59 (1990).
 - [20] A. Benyoussef, A. El Kenz, and T. Kaneyoshi, *J. Magn. Magn. Mat.* **131**, 173 (1994).
 - [21] A. Benyoussef, A. El Kenz, and T. Kaneyoshi, *J. Magn. Magn. Mat.* **131**, 179 (1994).
 - [22] A. Bobák and M. Jurin, *Physica A* **240**, 647 (1997).
 - [23] B. Deviren, M. Ertas, and M. Keskin, *Physica A* **389**, 2036 (2010).
 - [24] M. Ertas, E. Kantar, Y. Kocakaplan, and M. Keskin, *Physica A* **444**, 732 (2016).

- [25] I. J. Souza, P. H. Z. de Arruda, M. Godoy, L. Craco, and A. S. de Arruda, *Physica A* **444**, 589 (2016).
- [26] J. S. da Cruz Filho, T. Tunes, M. Godoy, and A. S. de Arruda *Physica A* **450**, 180 (2016).
- [27] J. S. da Cruz Filho, M. Godoy, and A. S. de Arruda, *Physica A* **392**, 6247 (2013).
- [28] J. A. Reyes, N. de La Espriella, and G. M. Buendía, *Phys. Status Solidi B* **10**, 252 (2015).
- [29] N. de La Espriella, C. A. Mercado, and J. C. Madera, *J. Magn. Magn. Mater.* **401**, 22 (2016).
- [30] S. G. A. Quadros and S. R. Salinas, *Physica A* **206**, 479 (1994).
- [31] G. M. Zhang and Ch. Z. Yang, *Phys. Rev. B* **48**, 9452 (1993).
- [32] G. M. Buendia and J. A. Liendo, *J. Phys.: Condens. Matter* **9**, 5439 (1997).
- [33] M. Godoy and W. Figueiredo, *Phys. Rev. E* **61**, 218 (2000).
- [34] N. Stanica, C. V. Stager, M. Cimpoesu, and M. Andruh, *Polyhedron* **17**, 1787 (1998).
- [35] J. R. V. Pereira, T. M. Tunes, A. S. de Arruda, and M. Godoy, *Physica A* **500**, 265 (2018).
- [36] M. Godoy, V. S. Leite, and W. Figueiredo, *Phys. Rev. B* **69**, 054428 (2004).
- [37] N. Metropolis, A. Rosenbluth, M. Rosenbluth, A. Teller, and E. Teller, *J. Chem. Phys.*, **21**, 1087 (1953).
- [38] K. Binder in *Finite-Size Scaling and Numerical Simulation of Statistical Systems*, edited by V. Priviman (World Scientific, Singapore, 1970).
- [39] W. Selke and J. Oitmaa, *J. Phys.: Condens. Matter* **22**, 076004 (2010).
- [40] Y. Nakamura and J. W. Tucker, *IEEE Transactions on Magnetics* **38**, No. 5 (2002).
- [41] M. Žukovič and A. Bobák, *Physica A* **389**, 5402 (2010).